

Atsuo Takahashi
Rio Kita
Takashi Shinozaki
Kenji Kubota
Makoto Kaibara

Real space observation of three-dimensional network structure of hydrated fibrin gel

Received: 25 October 2002
Accepted: 2 December 2002
Published online: 1 February 2003
© Springer-Verlag 2003

A. Takahashi · R. Kita (✉)
T. Shinozaki · M. Kaibara
RIKEN (The Institute of Physical
and Chemical Research), Wako,
351-0198, Saitama, Japan
E-mail: kita@mpip-mainz.mpg.de
Tel.: +49-6131-379248
Fax: +49-6131-379100

A. Takahashi
Department of Physics,
Faculty of Science,
Science University of Tokyo,
Shinjuku, 162-0825 Tokyo, Japan

K. Kubota
Department of Biological and Chemical
Engineering, Faculty of Engineering,
Gunma University, Kiryu,
376-8515 Gunma, Japan

Present address: R. Kita
Max-Planck-Institute for Polymer
Research, Ackermannweg 10,
55128 Mainz, Germany

Present address: T. Shinozaki
Department of Complexity Science and
Engineering, Graduate School of Frontier
Sciences, University of Tokyo, Bunkyo,
113-0033 Tokyo, Japan

Abstract The three-dimensional (3-d) network structure of the gel composed of rigid rod-shaped protein (fibrin gel) in a hydrated state was elucidated from a real space observation by confocal laser scanning microscopy. It was ascertained that two the length scales that characterize the gel network (diameter of polymer chain and typical mesh size of the gel network) can be determined quantitatively by a 3-d box-counting analysis and a 3-d Fourier transform (FT) analysis to obtain the power spectra. Turbidity measurements were employed for the determination of average fiber diameter. Self-similar structure of the gel network was found to be realized in the range between those two scales. The fibrin gels formed by larger amounts of thrombin showed a smaller fractal dimension that, deduced by the box-counting method, was in good agreement with the result from 3-d FT analysis and with a recent dynamic light scattering study (Kita R. et al. (2002) *Bio-macromolecules* 3:1013).

Keywords Fibrinogen · Fibrin · Gel · Network structure · Confocal laser scanning microscopy

Introduction

The network structure of gels and gelation processes have been studied in relation to the physicochemical aspects using various experimental approaches [1, 2, 3, 4,

5, 6]. Gel properties have been established by means of swelling behavior, rheological properties, scattering behaviors, and so on. Such approaches postulate, more or less implicitly, that the network structure should be sufficiently homogeneous. However, it has become

clear that the microscopic network structure is quite inhomogeneous due to the frozen network structure by gelation and that such a local inhomogeneity affects the macroscopic nature of the gel [4]. Therefore, the relationship between the local inhomogeneity and various macroscopic properties should be clarified at the molecular scale. However, the significance of local inhomogeneity has not yet been clarified.

Real space observation of the network structure is one of the direct approaches for studying the characteristics of gels. The knowledge of network structure at the elementary chain length scale can give insight into gel formation and properties without using the statistical average values. Many researchers have attempted to study the gel networks using scattering [1] and rheological measurements [2, 3]. These techniques are indeed powerful methods to study the network structure, although they yield averaged values for gels. Scanning electron microscope (SEM) is useful for observation of the network structure directly, but it may include some artifacts during sample treatments. Moreover, the use of SEM and atomic force microscopy (AFM) are restricted in observing the surface of samples as these methods can only observe the 2-dimensional structures.

Hirokawa et al. reported a direct observation of poly(*N*-isopropylacrylamide) gel using confocal laser scanning microscopy (CLSM) and constructed a 3-d structure of that gel [7]. Although they revealed the structural inhomogeneity of the gel, the observed images were not of the polymer network itself due to the limitation of the optical resolution, but they showed its domain structure with concentration fluctuation. Blombäck et al. also studied the properties of fibrin gel by CLSM and gave the polymer diameter and a permeability index in combination with the permeation and turbidity measurements, but quantitative analyses of the network structure were not carried out [8]. There are many theoretical and experimental studies on the physicochemical properties of gels and network structure [1, 2, 3, 4, 5, 6, 7, 8, 9, 10]. A self-similar structure of gel network on a specific time and space scale has been discussed using scaling theories based on a lattice percolation model [9, 11]. It should be mentioned that the characteristics of cross-linking (such as branching number at the cross-linking point, length of orientation of branching chains) are important features for studying the properties of gel network [6]. However, few studies have been reported on the 3-d network structure of gels deduced from direct observation at the molecular level, keeping the specimen in solvated states.

Fibrin, which is a rod-shaped polypeptide, is converted from fibrinogen by thrombin with a specific cleavage of small peptides. A spontaneous aggregation of fibrins (monomer unit) forms the fibrin gel and this gelling process has been studied extensively [12, 13, 14]. In the present study, a real space observation of fibrin

gels formed under different thrombin concentrations was performed with CLSM in order to investigate the 3-d network structure of hydrated fibrin gels. By correcting the fiber diameter using turbidity measurements, the network structure was determined free from the blurring by fluorescent light. The sparse network structure of fibrin gel was clearly demonstrated. The results are also analyzed by a fractal concept, because a self-similar structure of gels is one of the important parameters for characterizing the network structure [14]. The reason for selecting the fibrinogen–thrombin solution to study the gel network structure is that the diameter of networking chain and the mesh size of the network are on the micrometer scale. These characteristics are suitable for the direct observation of network using CLSM [8]. The present techniques make it possible to analyze the characteristics of cross-linkages of rigid rod-like polymers and the process of network formation, including growth of fibers and branching.

Experimental

Bovine fibrinogen (clottability 97%), from Sigma-Aldrich, was dissolved in a 0.15 M phosphate buffer solution (PBS) at pH 7.4. The final fibrinogen concentration of 0.22 g/100 mL was used for all measurements. The solutions were gelled by adding bovine thrombin with a final concentration of 0.02 NIH units/mL (sample A) and 0.00125 NIH units/mL (sample B). Sample A had faster gelation kinetics compared to sample B and the gelation dynamics of these samples was studied in detail in a recent report [14]. In order to carry out the CLSM measurements on the equilibrium state of fibrin gels, 100 μ L of sample solutions were poured into dishes, with a glass bottom of 120 μ m depth, immediately after fibrinogen and thrombin were mixed. The dishes were capped and incubated at 37 °C for more than 5 h (samples A) and 12 h (sample B) to accomplish complete gel formation. Then, the fibrin gel networks were stained by pouring 3 mL of 0.17 mM fluorescein isothiocyanate (FITC) in 0.15 M PBS (pH 8.0) into the dishes and leaving for about 12 h. They were washed thoroughly with fresh PBS to remove excess FITC for about 24 h. In order to prevent photo-bleaching of FITC, 50 mM of *p*-phenylenediamine was percolated into the fibrin gel by adding it to the fresh buffer [15].

A confocal laser scanning microscope (LSM510, Carl Zeiss, Germany) was used to obtain the sliced images. An Ar-ion laser, with wavelength 488 nm, was used for the excitation of FITC. The emission of 505–530 nm from FITC was detected through a filter system. The 256 images focused on the *z*-axis plane were stacked in every 0.1 μ m depth in the *z*-axis. The observed areas of CLSM were randomly chosen for the respective samples and consisted of 25.6 \times 25.6 \times 25.6 μ m with the resolution of 512 \times 512 \times 256 pixels. Eight sets of 3-d images were obtained for each sample and all measurements were averaged for each of these eight sets. Resultant 3-d images were more blurred in the *z*-direction than in the *x*- and *y*-direction because the resolution in focal depth is smaller than in the *xy*-plane. In order to reduce this effect, we assumed a point spread function and performed a deconvolution on the images. The real averaged fiber diameters were adopted as the threshold values to obtain the binarized images, which were determined by the turbidity measurement as a function of wavelength λ according to Carr et al. [16].

The binarized images were used to analyze the network structure. The distribution of the fiber diameter was obtained by the procedure that several sizes of spheres were fitted to cover the

sectional area of all fibers. Also, the network structure was analyzed using a 3-d box-counting method [17, 18] and a 3-d Fourier transform (3d-FT). In the 3-d box-counting method, 3-d images are divided into smaller cubes of certain size and the fractal dimension D_f of objects (gel network) is defined as

$$N(R) \sim R^{D_f} \quad (1)$$

where R is the cube size (length) that divides the whole observed region and $N(R)$ is the number of the cubes with size R that contains any part of the objects. Since the source data is a digitized image, the whole image size L cannot always be divisible by R . In such a case, we distribute the cubes randomly and $N(R)$ was calculated as follows:

$$N(R) = (L/R)^3 N'(R) / N_t \quad (2)$$

where N_t is the total number of randomly distributed cubes and $N'(R)$ the number of cubes that contain any parts of the objects among N_t cubes. N_t was set in the order of $(L/R)^3$ or more. Homemade programs were used in all the procedures, and the reliability of the program was verified by using simple lines and Koch curve. A power spectrum of the 3-d image, $P(u, v, w)$, was calculated as

$$P(u, v, w) = |F(u, v, w)F^*(u, v, w)| \quad (3)$$

where $F(u, v, w)$ is the Fourier transform of the original image and $F^*(u, v, w)$ is the complex conjugate of the Fourier transform. $P(u, v, w)$ is proportional to the scattered light intensity by normalizing with $k = (u^2 + v^2 + w^2)^{1/2}$. Here, $u, v,$ and w are the spatial frequency in the x -, y -, and z -directions, respectively [19].

Results and discussion

Figure 1 shows a typical observation of the 2-d sliced image of the fibrin gel network (sample A). The inside of

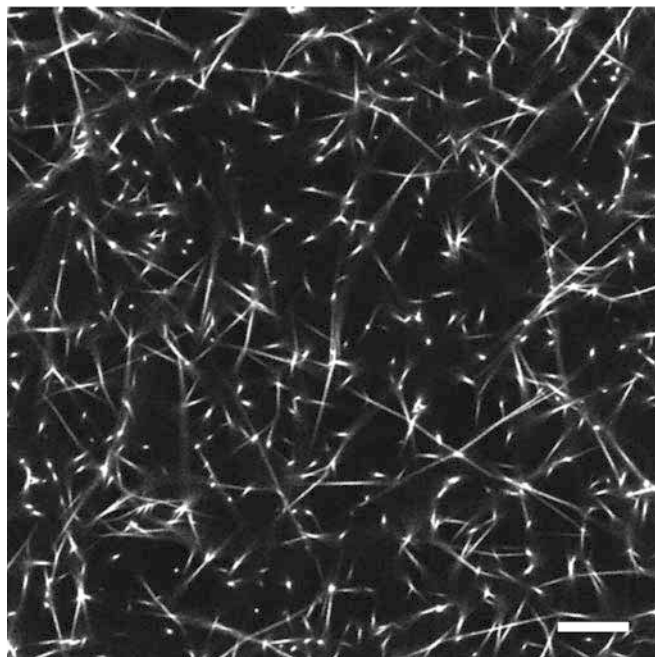


Fig. 1 Sliced image of the network structure of fibrin gel in the hydrated state for sample A. The *bar* indicates 10 μm

the network structure could be observed clearly in the hydrated state. The bright lines correspond to the polymers (fibrin fibers) that are parallel, relative to the sliced interface, and the bright spots indicate the fibrin fibers crossing the interface. Because it was observed that fibrin(ogen) adsorbed on the glass surface and formed a different network structure from the bulk structure, we measured only the images more than 20 μm apart from the glass surface to avoid such an effect.

Figure 2 shows the 3-d images constructed from the stacked sliced images and also the typical 2-d source images. It can be observed that sample A has a denser network consisting of fine fibers with a shorter cross-linking distance. On the other hand, the slowly grown gel (sample B) with a smaller amount of thrombin has a sparser network consisting of coarse fibers and a longer cross-linking distance. These structural images are consistent with the previous study [20]. Detailed structure of the cross-linking point of fibrin gel has remained a problem, since judgments of the cross-linking point are difficult on a sliced image [8] (as can be seen in Fig. 1) and SEM images. The present 3-d images can reveal the

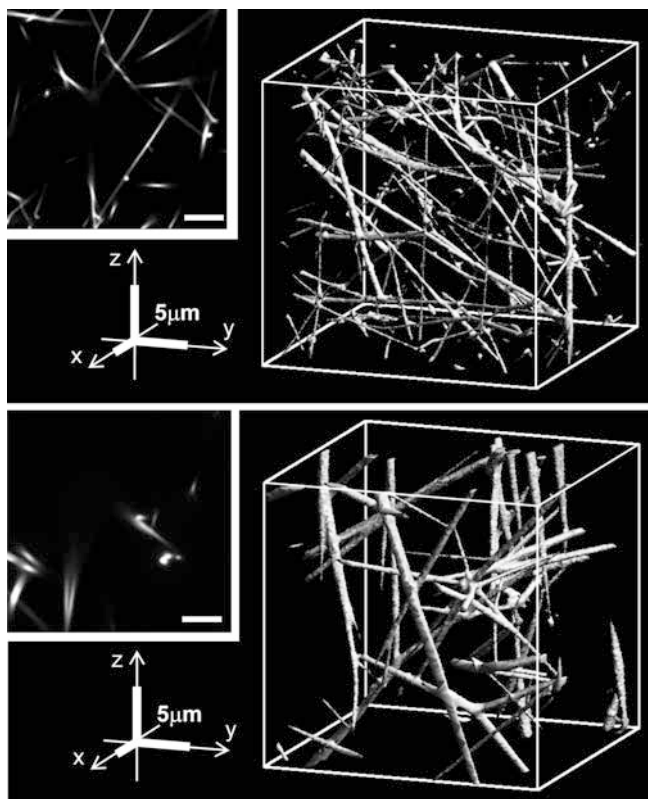


Fig. 2 Typical source images (*small figures*) and 3-d images constructed from the stacked sliced images for sample A (*top*) and sample B (*bottom*). The *bars* in the sliced images and the *bold lines* on x -, y - and z -axis indicate the length as 5 μm

existence of the cross-linking points clearly. It seems that multiplicity of branching from the cross-linking points is not extensive.

The histograms of fiber diameter distribution determined by the 3-d images are illustrated in Fig. 3. The average fiber diameters, d , determined by turbidity measurements as $d=0.11\ \mu\text{m}$ (sample A) and $d=0.16\ \mu\text{m}$ (sample B) are also shown as arrows. The width of the bar in the histogram corresponds to 1 pixel, i.e., $0.05\ \mu\text{m}$. Sample A showed a relatively sharper distribution with a smaller average fiber diameter. On the other hand, sample B showed a broader distribution without a distinct peak. These characteristics may closely relate to the gelling mechanism. The typical mesh sizes of the gel network, which were determined by the 3-d box-counting analysis mentioned below, were 4.9 and $11\ \mu\text{m}$, for samples A and B, respectively. These typical mesh sizes are ca. 50 and 70 times larger than the average fiber diameters for samples A and B, respectively. The result clarifies the sparse network structure of fibrin gel quantitatively. Although computer analysis for specifying the cross-linking point is still difficult, quantitative analyses are now in progress on the important parameters such as the distribution of branching number, the number density of cross-linking points, the length between cross-linking points, and so on.

Figure 4 shows the double logarithmic plots of $N(R)$ as a function of R as the results of the 3-d box-counting method for samples A and B. $N(R)$ can be divided into

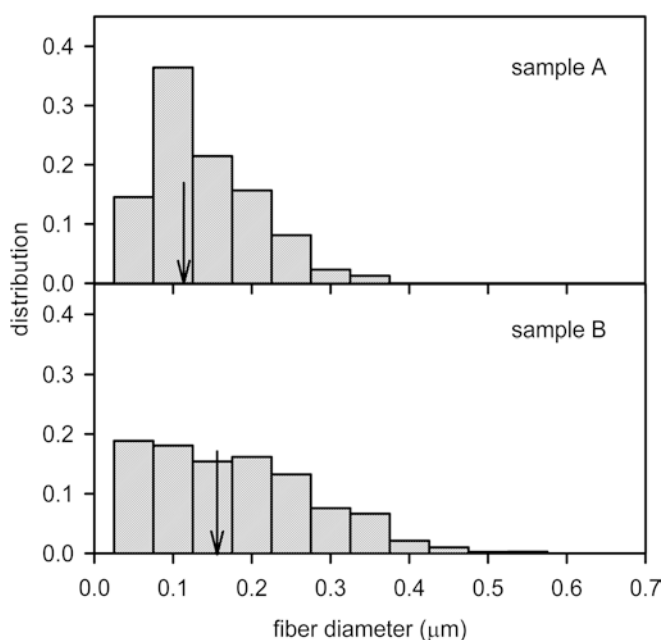


Fig. 3 Histograms of normalized distribution of the fiber diameter for samples A and B. The arrows indicate the average fiber diameters, determined by turbidity measurements, which correspond to 0.11 and $0.16\ \mu\text{m}$ for samples A and B, respectively

three regions. In the central region, a power law behavior was observed and the slope of the power law was above 3 and not an integer. This result indicates that the network structure has a self-similar nature and a fractal one. The fractal dimension, D_f , was obtained by a least squares fit to Eq. 3 at the central region as $D_f = 1.46 \pm 0.01$ and 1.54 ± 0.02 for samples A and B, respectively. Here, \pm denotes one standard deviation. These values are in agreement with those obtained by the dynamic light scattering measurements, 1.42 and 1.53 for the samples A and B, respectively [14]. The double logarithmic plot of $N(R)$ vs. R should have the slope of -3 where the cube size R is below 1 pixel and above 512 pixels, because all boxes at those R must contain the objects. Then, the straight lines having the slope of 3 and passing the data points of $R=0.05\ \mu\text{m}$ (1 pixel) or $R=25.6\ \mu\text{m}$ (512 pixels) were drawn in Fig. 4. These two lines cross the regression lines, and the crossing points are considered to be the average fiber diameters d_A and d_B and also the characteristic mesh sizes of networks S_A and S_B . Here, the subscripts A and B refer to the samples A and B, respectively. The reason for this assumption is that the network structure behaves as a mass fractal between these two length scales and the system should be regarded as a 3-d object in the scales below the fiber diameter and above the mesh size. The crossing points were $d_A=0.12\ \mu\text{m}$ and $d_B=0.15\ \mu\text{m}$,

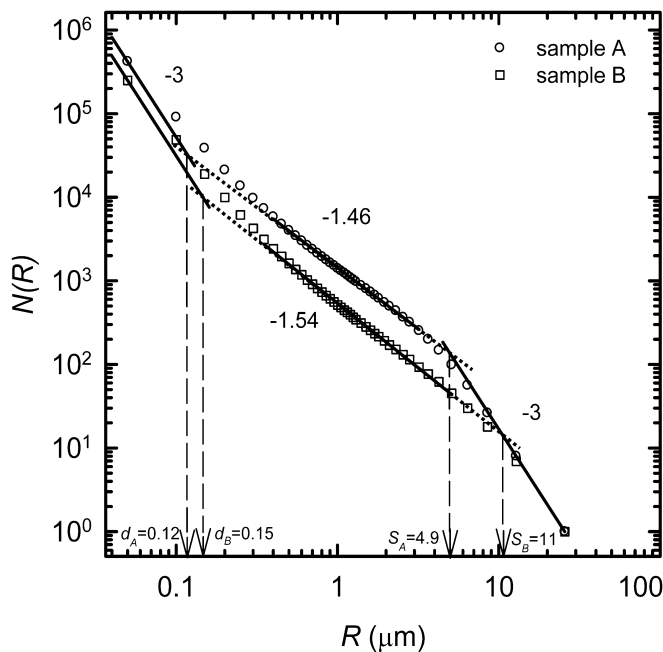


Fig. 4 Double logarithmic plots of $N(R)$ vs. R for the samples A (\circ) and B (\square). In the central region, samples A and B have slopes of 1.46 and 1.54 , respectively, which were determined by a least squares fitting using the data range $0.4 \leq R \leq 3.2\ \mu\text{m}$ for sample A and $0.35 \leq R \leq 5.1\ \mu\text{m}$ for sample B. The dashed lines were extrapolated to the regression lines

which were in good agreement with the average fiber diameters determined by the turbidity measurements. The typical mesh sizes evaluated by the crossing points were $S_A = 4.9 \mu\text{m}$ and $S_B = 11 \mu\text{m}$. These results indicate that a slow gelation process (sample B) yields a relatively sparse network structure, as can be seen in the 3-d images (Fig. 2). Fibrin gel formation proceeds in a stepwise manner: that is, in the first step fibrin and protofibril are formed from fibrinogen and, in the succeeding step, the lateral aggregation of protofibrils forms fibrin fibers and these form a three dimensional network consisting of fibers [14]. Protofibrils develop well in the first step, interact, and form the embryo of the gel network. Succeedingly, the network structure develops together with the lateral aggregation (growth). In the slow gelation process, rearrangement of mobile fibrin fibers is likely to occur and the lateral growth of fibrin fibers proceeds well. This rearrangement may effectively result in a larger mesh size. It should be mentioned that further studies are required to confirm whether the observed power law behavior is the real nature of the gel or an apparent nature in terms of the box-counting method.

Figure 5 shows the double logarithmic plots of the normalized power spectra $P(k)$ of the averaged radial distribution function as a function of wavenumber k determined by 3-d FT, for samples A and B. In the very high frequency range corresponding to the average fiber diameter, it is expected that the Porod law should hold [21]. However, in our experimental condition, it could not be observed because of the restriction of image resolution. The appearance of the peak in $P(k)$ indicates

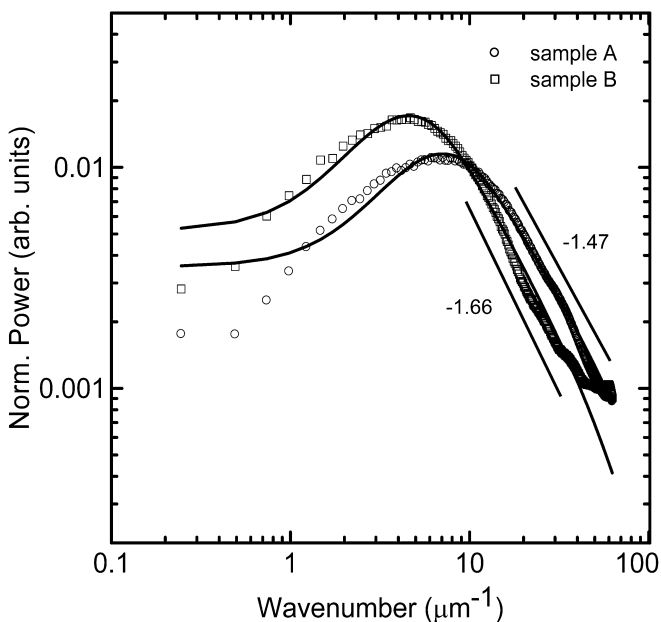


Fig. 5 Double logarithmic plots of the normalized power spectra $P(k)$ vs. wavenumber k for samples A (○) and B (□). The solid curves are the fitted function (see text)

the existence of a characteristic length of network structure. Furthermore, in the region greater than the peak wavenumber (but lower than the maximum wavenumber $20\pi \mu\text{m}^{-1}$), the power law behavior of the spectra against the wavenumber $P(k) \sim k^{-D}$ holds well suggesting the self-similar structure of the network. The fractal dimension relates to the power law exponent. The fractal dimensions were obtained as 1.47 ± 0.05 and 1.66 ± 0.05 for the samples A and B, respectively, in agreement with the results by the box-counting method.

The solid curves in Fig. 5 are the fitted functions derived by Ferri et al. [21]. Fairly good fittings were obtained. Ferri et al. assumed a spatial structural factor and a form factor for the case that the cylindrical segments, with diameter d and length l , bonded together in an end-to-end manner and a blob, of length of ξ , is made of assembly of segments. Moreover, they assumed a self-similar structure of the fibrin gel. According to their formulation, the scattered intensity $R(k)$ as a function of k is described as

$$R(k) = KcM \{1 - \beta \exp[-(\gamma \xi k)^2]\} \{1/[1 + (k\xi/\pi)^2]^{(D/2)} + (l/\xi)^D \{1/[1 + k^2 d^2 (l/32d)^{1/2}]^{(\alpha/2)}\} \quad (4)$$

Here, β is the parameter that controls the correlation amplitude of structure factor, α , the exponent by which the power law behavior of the system is characterized at the frequency range above the wavenumber corresponding to the diameter of cylindrical segments. D is the fractal dimension of network structure. K , c and M are the optical constant, concentration, and molecular weight, respectively. The fractal dimensions of D from the fitting were $D = 1.40 \pm 0.02$ and $D = 1.53 \pm 0.02$ for samples A and B, respectively. These values are consistent with those evaluated from the k -dependence of power spectra (1.47 and 1.66). Here, we assumed that $l = d = 0.03\xi$, tentatively according to Ferri's results, and ξ was $3.61 \mu\text{m}$ and $5.34 \mu\text{m}$ for samples A and B, respectively. When d is fixed at 0.11 and $0.16 \mu\text{m}$ for samples A and B, respectively, ξ values were $3.75 \mu\text{m}$ and $5.64 \mu\text{m}$ and D values were 1.45 and 1.50 . The fitting for the sample A looks better than B. This could be due to the fact that the sample B has a rather sparse network structure and, therefore, the statistical averaging based on the observed area by CLSM pictures is still not sufficient. The characteristic lengths corresponding to the peak position are ca. 3.7 and $5.9 \mu\text{m}$ for the samples A and B, respectively, according to the relation $\xi \sim 4.4/k_1$, pointed out by Ferri (with k_1 being the peak wavenumber). These values are in agreement with the values of ξ obtained by the fitting.

Ferri et al. also showed the existence of three different regimes delimited by two wavevectors k_1 and k_2 , which corresponded to the average gel blob size and the average fiber size, respectively, based on the behavior of the scattered light intensity as a function of k using low

angle elastic light scattering. Furthermore, in the range $k_1 < k < k_2$, a power law behavior was obtained and the fractal dimension D was determined as 1.3 [21]. Their experimental conditions were different from our study in the temperature and thrombin concentration. The thrombin concentration in their experiment was about 1 NIH units/mL, which was much higher than for sample A. However, these results imply that more rapid gelation in fibrin gels at higher thrombin concentration tends to give smaller D .

In a silica gel, Martin et al. first reported the fractal dimension deduced from the power law behavior of the time correlation function by dynamic light scattering [22]. The fractal dimension was determined by the slope of the double logarithmic plots of the correlation function as a function of the delay time, which implies that the power law decay of the correlation function results from a self-similar nature of the cluster forming the gel network. Shibayama et al. also carried out the dynamic light scattering study for the gelling systems and showed the relationship between the power law exponents and the network structure [23]. Usually, the fractal dimension of gels tends to show a larger value when they are composed of flexible chains and more branching numbers [24]. It should, however, be noted that the meaning of the equivalence between the mass fractal dimension and the fractal dimension determined by the power-law exponent of the correlation function has not been well provided theoretically and there still remain controversial problems [23, 24, 25, 26]. The relatively good agreement of the fractal dimensions evaluated by the 3-d box-counting method, power law behavior of power spectra, and fitting of power spectra by Ferri's function with the time correlation function of our recent study by dynamic light scattering, suggests the validity of dynamic light scattering for the evaluation of the fractal dimension.

The sample A, which has a larger thrombin concentration than the sample B, shows a smaller fractal dimension. It may simply be that when the mesh size and fiber diameter are smaller and the distribution of the fiber diameter is narrower, the result is a denser spatial filling and a higher fractal dimension. However, this is not the present case where the stepwise conversion of fibrinogen proceeds to fibrin gel. The present results suggest that the orientational ordering of the gel formed by rigid fibrin fibers may effectively affect the spatial filling and the fractal dimension. In fact, Lidar et al. showed that when rods are randomly distributed with isotropic orientation, fractal dimension depends essentially only on the coverage of rods. Further, when anisotropically oriented rods are randomly distributed, the fractal dimension depends not only on the coverage but also on the degree of anisotropy, and the fractal dimension decreases with the rods becoming more parallel [27]. Indeed, the orientational ordering seems to be more anisotropic in sample A, in accordance with the Lidar's

results. It is very necessary to evaluate the orientational order quantitatively based on the real space observation.

It has been reported that the structure of fibrin network varies continuously between fine and coarse clot, affected by many factors [28]. In the present paper, the network structure of fibrin was examined under two different thrombin concentrations. To understand the network structure of fibrin fully, it is necessary to observe the network structure of clots formed under different conditions, including pH, ionic strength, and the concentration of fibrinogen. Such a study will be reported in the near future.

Fibrinolytic and hemostatic kinetics of blood and various properties of clots (such as mechanical strength, syneresis, opacity, and clot retraction) are associated with the structural characteristics of fibrin networks. For example, remarkable syneresis in fibrin gels should be correlated with the sparse network consisting of rigid rod fibers and low multiplicity of branching at the cross-linking point. The analysis of network structure, which is represented by fractal dimension, mesh size and orientational ordering, may be useful for understanding the physiological phenomena as well as physical properties of clots formed under various physiological conditions.

Conclusion

The CLSM measurement, as a real space observation, was carried out for fibrin gel in a hydrated state and revealed the 3-d network structure of fibrin gel at the molecular scale. The characteristics of the structure were analyzed by digital image processing. The existence of two characteristic length scales was ascertained by 3-d box-counting. Moreover, the 3-d box-counting method yielded the fractal nature of fibrin gel in the scale between the fiber diameter and typical mesh size of the gel, and the fractal dimension D_f was evaluated. The 3-d FT analysis was also carried out for the same real space images to obtain the power spectrum. A self-similar nature was observed in this spectrum and the fractal dimension was evaluated by the wavelength dependence. The power spectrum was also analyzed using Ferris scattering function and gave the fractal dimension. The obtained fractal dimensions from the individual analyses showed good agreement with each other. The present results justify the evaluation of the fractal dimension by the correlation function measurements. Further study on the orientational order is important and necessary for the detailed understanding of gels formed by rigid polymers.

Acknowledgment We acknowledge Dr. T. Kobayashi and Ms. K. Ishii of RIKEN for their advice on the experiment of the CLSM and Dr. M. Takemasa of Waseda University for helpful discussions about computer programming.

References

1. Freltoft T, Kjems JK, Sinha SK (1986) *Phys Rev B* 33:269
2. Martin JE, Adolf D, Wilcoxon JP (1988) *Phys Rev Lett* 61:2620
3. Shih WH, Shih WY, Kim SI, Liu J, Aksay IA (1990) *Phys Rev A* 42:4772
4. Tokita M, Tanaka T (1991) *J Chem Phys* 95:4613
5. Kaibara M (1994) *Polym Gels and Networks* 2:1
6. Tanaka F (2000) *Macromolecules* 33:4249
7. Hirokawa Y, Jinnai H, Nishikawa Y, Okamoto T, Hashimoto T (1999) *Macromolecules* 32:7093
8. Blombäck B, Carlsson K, Hessel B, Lilgeborg A, Procyk R, Aslund N (1989) *Biochim Biophys Acta* 997:96
9. Stauffer D (1976) *J Chem Soc Faraday Trans* 272:1354
10. Muthukumar M (1983) *J Chem Phys* 83:3161
11. Stauffer D (1985) *Introduction to percolation theory*. Taylor & Francis, London
12. Weisel JW (1986) *Biophys J* 50:1079
13. Kaibara M (1996) *Biorheology* 33:101
14. Kita R, Takahashi A, Kaibara M, Kubota K (2002) *Biomacromolecules* 3:1013
15. Platt JL, Michael AF (1988) *J Histochem Cytochem* 31:840
16. Carr ME, Hermans J (1978) *Macromolecules* 11:46
17. Farmer JD, Ott E, Yorke JA (1983) *Physica D* 7:153
18. Rothschild WG (1998) *Fractals in chemistry*. Wiley, New York
19. Tanaka H, Hayashi T, Nishi T (1986) *J Appl Phys* 59 3627
20. Ryan EA, Mockros LF, Weisel JW, Lorand L (1999) *Biophys J* 77:2813
21. Ferri F, Greco M, Arcovito G, Bassi FA, DeSpirito M, Paganini E, Rocco M (2001) *Phys Rev E* 63:31401
22. Martin JE, Wilcoxon JP (1988) *Phys Rev Lett* 61: 373; Martin JE, Wilcoxon JP, Odinek J (1991) *Phys Rev A* 43:858
23. Norisuye T, Shibayama M, Tamaki R, Chujo Y (1999) *Macromolecules* 32:1528; Takata S, Norisuye T, Tanaka N, Shibayama M (2000) *Macromolecules* 33:5470
24. Adam M, Lairez D (1996) *Sol-gel transition* In: Addad JPC (ed) *The physical properties of polymeric gels*. Wiley, New York, pp 87–142
25. Ren SZ, Shi WF, Zhang WB, Sorensen CM (1992) *Phys Rev A* 45:2416
26. Doi M, Onuki A (1992) *J Phys II (France)* 2:1631
27. Lidar DA, Biham O, Avnir D (1997) *J Chem Phys* 106:10359
28. Ferry JD, Morrison PR (1947) *J Am Chem Soc* 69:388